Journal of the Ceramic Society of Japan 117 [6] 732-735 2009 **Paper**

Bipolar resistance switching property of Al–Ag/$La_{0.7}Ca_{0.3}MnO_3$/Pt sandwiches

Xin Jun LIU,[*] X. M. LI,[*] W. D. YU,[*] Q. WANG,[*] R. YANG,[*,] X. CAO[*,**] and L. D. CHEN[*,†]**

[*]**State Key Laboratory of High Performance Ceramics and Superfine Microstructures, Shanghai Institute of Ceramics, Chinese Academy of Sciences, Shanghai 200050, People's Republic of China**

[**]**Graduate School of the Chinese Academy of Sciences, Beijing 100039, People's Republic of China**

Bipolar resistance switching was investigated on $La_{0.7}Ca_{0.3}MnO_3$ (LCMO) thin film with Al–Ag alloy top electrode (TE) including different Ag contents. The switching capability of Al–Ag/LCMO/Pt was greatly improved in Al-33%Ag TE structure compared to in Al-50%Ag TE structure. Switching times of faster than 100 ns and rewrite cycles of more than 400 were obtained while maintaining a ratio of resistance change larger than 1000%. The mechanism of resistance switching was explained by a model with interfacial nanostructured domains composed of Ag and insulator AlO_x matrix, as previously proposed for Al-50%Ag/LCMO/Pt structure.

Key-words : RRAM, Resistance switching, Alloy electrodes, Manganites, Thin film

[Received December 8, 2008; Accepted February 19, 2009]

1. Introduction

In recent years, the electric-pulse-induced resistance switching (EPIR) phenomena in metal oxides have attracted considerable research interest due to their potential application to resistance random access memory (RRAM), which is considered as the promising next-generation nonvolatile memory with some advantages of drastically reduced power consumption, fast switching speed and nondestructive readout.[1)–16)] Bipolar resistance switching (RS), characterized by the different voltage polarities for the resistance state transitions, has been observed in perovskite manganites such as $Pr_{0.7}Ca_{0.3}MnO_3$ (PCMO) and $La_{0.7}Ca_{0.3}MnO_3$ (LCMO).[3)–16)] In terms of RS directionality, there are two kinds of bipolar EPIR switching phenomena, namely *positive* EPIR and *negative* EPIR.[11)] The former means the high resistance state (HRS) can be written by positive voltage pulses, and the low resistance state (LRS) can be reset using negative voltage pulses. Here, the *positive* voltage direction is defined as the current flowing from the top electrode (TE) to the bottom electrode (BE). Typical sandwiches with *positive* EPIR include Au/PCMO/Pt,[3)] Ag/PCMO/Pt,[4),5)] Mo/LCMO/Pt.[6)] In the latter, the switching voltage polarity is just the opposite from that in the *positive* EPIR effect. Typical sandwiches with *negative* EPIR include Al/PCMO/Pt,[7)] Ti/PCMO/Pt,[8)] Ta/PCMO/Pt,[9)] Sm/LCMO/Pt,[10)] In/PCMO/Pt[11)] sandwiches. Since same Pt BE and similar characteristic PCMO/LCMO were used in these experiments, a strong influence of the TE material on the polarity of bipolar EPIR were clearly indicated.

Furthermore, the switching speed is also strongly affected by the TE material and less affected by the BE material. When a noble metal like Ag or Au is used as the TE, the switching speed is fast, on the order of 100 ns or less.[3),4)] On the other hand, when an easily oxidized metal like Ti or Al is used, the switching speed is quite slow, on the order of 1 ms.[12),17)] In our recent research, Al-50%Ag alloy TE has been developed to realize the resistance switching of a noncrystalline and low-resistance LCMO thin film,[18)] and *positive* EPIR has been found in Al-50%Ag/LCMO/Pt structure. Meanwhile, under the applied pulses of ±10 V magnitude and as long as 10 μs duration, the average ratio of resistance change $(R_{HRS}-R_{LRS})/R_{LRS} \times 100\%$ is around 120%, which can meet the need of practical applications for RRAM. It is clear that the polarity of bipolar EPIR for Al-50%Ag/LCMO/Pt structure is same as that of bipolar EPIR for Ag/LCMO/Pt structure,[4)] while the switching speed for Al-50%Ag/LCMO/Pt structure is rather close to that for Al/LCMO/Pt structure.[7)] Therefore, by changing the Ag content in the Ag–Al alloy electrodes, it is expected to obtain more fast switching speed while remain the high-initial-resistance property. In this paper, Al-33%Ag/LCMO/Pt structure was prepared and *positive* EPIR was observed. The observed switching property is better than that in Al-50%Ag/LCMO/Pt structure.[18)] Under the applied pulses of ±5 V magnitude and as low as 100 ns duration, the ratio of resistance change is more than 1000% and switching cycle is larger than 400.

2. Experiments

The LCMO films were prepared by the pulse laser deposition (PLD) method on Pt/Ti/SiO_2/Si substrates, as described previously.[18)] The oxygen pressure during the deposition was kept at 1 Pa with the substrate temperature (T_s) of 550–650°C. The thickness of the LCMO film is around 300 nm. The composition of the thin film is in close agreement with that of the target. Al and Ag layers were respectively deposited by electron beam evaporation and thermal evaporation under a base vacuum of $< 5 \times 10^{-4}$ Pa and a T_s of 200°C. The Al-33%Ag alloy electrode, with 100 μm in diameter and 200 nm in thickness, was fabricated by simultaneously employing above procedures with the different deposition rate to keep the Al and Ag atomic ratio of 2:1. Electrical measurements were conducted by two-probe method using a dc source meter (Keithley 2410-c) and a pulse generator (Agilent 81104A). The resistance was measured by applying a 1 μA dc current and reading the corresponding voltage across the film after each bias scan or voltage pulse. All the measurement

† Corresponding author: L. D. Chen; E-mail: cld@mail.sic.ac.cn

was performed at room temperature (RT).

3. Results and discussion

Figure 1(a) shows typical X-ray diffraction (XRD) patterns for the LCMO films grown on (111)-oriented platinized silicon substrates with T_s = 550, 600 and 650°C. The films deposited at higher T_s show preferred (020)/(112) orientation, but no obvious peaks is found in that deposited at 550°C. Figure 1(b) presents a cross-sectional scanning electron microscope (SEM) image of a LCMO thin film grown at 550°C for 120 min. The LCMO layer exhibits no evident grain boundaries, which is also consistent with the XRD results shown above, indicating that the film is noncrystalline. The LCMO thin films used in the following electrical measurements are those grown at 550°C, therefore are of noncrystalline characteristic.

To find the proper pulse parameters, resistance hysteresis switching loop (HSL) were measured by applying a sequence of pulses with a constant voltage step. As an example, increasing negative pulses are applied when the sample was in the LRS until it switched to HRS. Then the pulse magnitude is reduced until it changes polarity to positive after which the magnitude is increased until the sample switches back to the LRS. For the sample of **Fig. 2**(a), at the threshold voltages of approximately +4 V and –4 V, the EPIR device resistance begins to switch to its LRS and HRS, respectively.

A measurement result of non-volatile static resistance versus electrical pulse number with the Al-33%Ag/LCMO/Pt structure is shown in Fig. 2(b), in which the pulse duration and amplitude were 100 ns and ±5 V, respectively. A positive pulse causes a decrease in resistance from HRS to LRS. The EPIR switching-reading process is reproducible from cycle to cycle and can continue for > 400 switch cycles as shown in Fig. 2(b), with however, some fatigue resulting in $\Delta R/R$ decreasing after the 400 cycles. Furthermore, a room temperature EPIR ratio as large as 1100% has also been obtained in the Al-33%Ag/LCMO/Pt structure in Fig. 2(b). **Table 1** shows the comparison of the selected RS performances between the Al-33%Ag/LCMO/Pt structures (this work) and other relative systems reported in the previous publications. It can be seen that an excellent over-all switching performance was achieved in the Al-33%Ag/LCMO/Pt structures.

I–V characteristic was measured by voltage swept as $0 \rightarrow +V_{max} \rightarrow 0 \rightarrow -V_{max} \rightarrow 0$. *I–V* plots between ±2 V and ±2.5 V are also shown in **Fig. 3**(a), similar to that of the Al-50%Ag/LCMO/Pt.[18] It can be seen that the resistance decreases under the positive voltage sweep and increases under the negative voltage sweep, which is similar to that of the Ag electrode[5] and opposite to that of the Al electrode.[7),17] These results indicate that the electron transport is carried by Ag in the Al-33%Ag electrode and the increase in the original resistance is induced by Al in it. So, this *I–V* characteristic can also be explained by carrier injected space charge limited conduction controlled by interface trapping/detrapping.[5] However, as voltage increases, a typical oxide film device will have a tendency to breakdown with considerable damage, as shown in Fig. 3(a).

Although various switching models have been proposed to explain resistance switching, the microscopic nature of resistance switching and charge transport in such structures is still under debate. A model with interfacial nanostructured domains composed of Ag and insulator AlO_x matrix was proposed to explain the characteristics of the Ag–Al alloy electrode TE sample.[18] Fig. 3(b) shows the schematic diagram of the interface layer

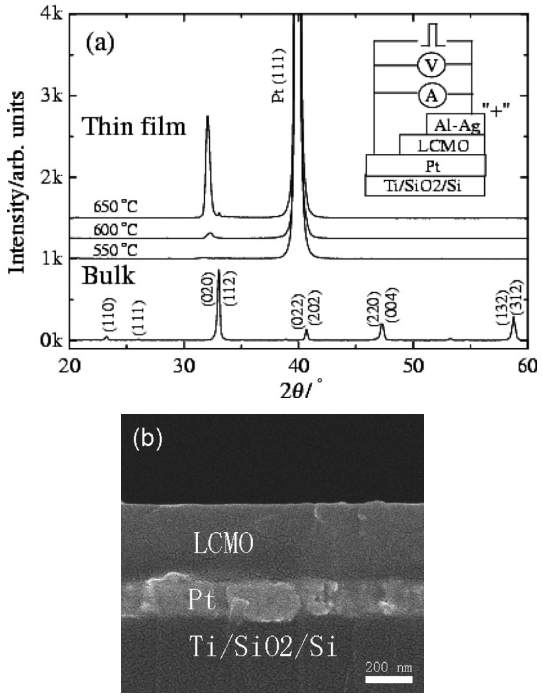

Fig. 1. (a) Typical XRD patterns for the $La_{0.7}Ca_{0.3}MnO_3$ films grown on Pt/Ti/SiO_2/Si substrates with T_s = 550, 600 and 650°C. (b) cross-sectional SEM image for the film grown at 550°C for about 120 min.

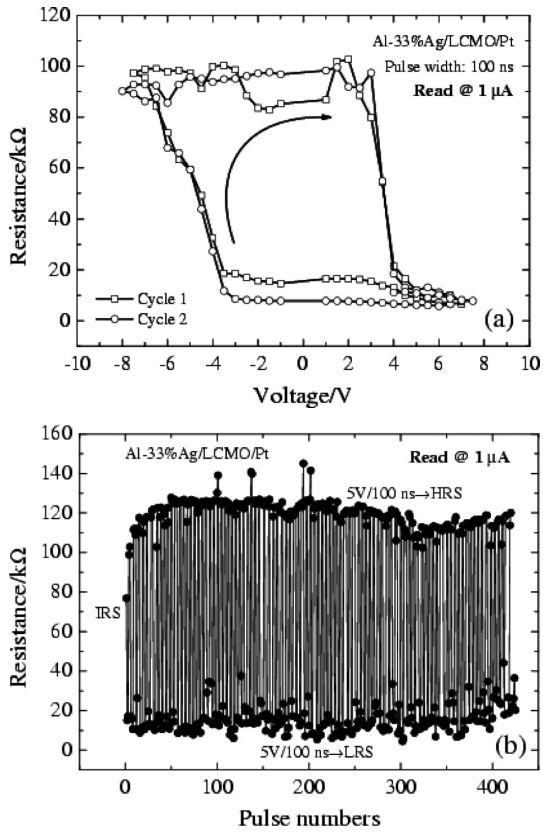

Fig. 2. (a) Resistance hysteresis switching loop for a LCMO sample. (b) EPIR fatigue performance of a LCMO sample under ±5 V and 100 ns pulses.

Table 1. Resistance Switching Performances of Al-33%Ag/LCMO/Pt Structure Comparison with Other Relative Structures

Structure	Voltage	Width	R_{HRS}	R_{LRS}	EPIR ratio	Reference
Ag/PCMO/$YBa_2Cu_3O_{7-x}$	±18 V	100 ns	3.5 kΩ	200 Ω	~1770%	4)
Ag/PCMO/Pt	±10 V	100 ns	800 Ω	550 Ω	~45%	19)
Ag/PCMO(O-rich)/Pt	+5/–6 V	200 ns	530 Ω	310 Ω	~70%	14)
Ag/PCMO(O-deficient)/Pt	±5 V	200 ns	36 kΩ	6 kΩ	~500%	14)
Ag paster/LCMO/Pt	±15 V	100 ns	100 kΩ	400 Ω	~10^5%	20)
Ag paster/PCMO/Pt	±1.6 V	500 ns	500 MΩ	500 kΩ	~10^5%	21)
Al-33%Ag/LCMO/Pt	±5 V	100 ns	120 kΩ	10 kΩ	~1100%	This work
Al-50%Ag/LCMO/Pt	±10 V	10 μs	1.3 kΩ	600 Ω	~120%	18)
Al/PCMO/Pt	±4 V	50 ns	38 Ω	23 Ω	~65%	7)
Al/PCMO/$LaNiO_3$	+5/–7 V	5 ms	1 MΩ	10 kΩ	~10^4%	17)

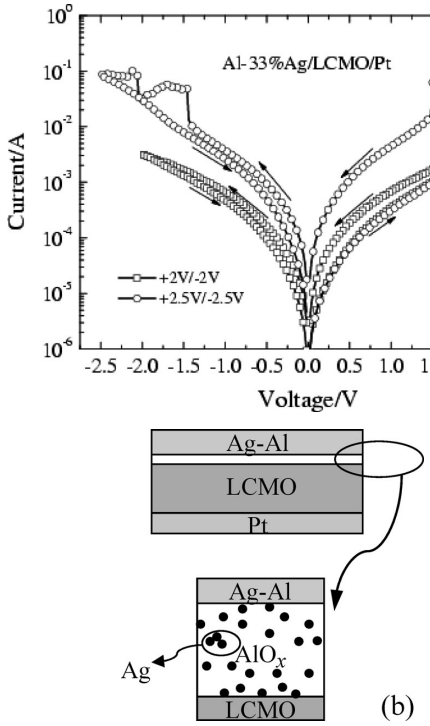

Fig. 3. (a) *I–V* characteristic of Al-33%Ag/LCMO/Pt structures in semi-log plots. (b) Schematic diagram of the interface layer between the Ag–Al alloy electrode and the LCMO film.

between the Ag–Al alloy electrode and the LCMO film. This Ag-contained AlO_x layer can be formed by the oxidation of Al not only during the alloy electrode deposition but also during the electrical scan or applied pulse. Due to the introduction of inert Ag, stable Ag conductive paths (filaments) will be created in the AlO_x matrix by a percolation effect. The formation of Ag filaments results in the point contacts between Ag–Al alloy TE and the LCMO film, which is similar to that of the Ag paste sample where the Ag particles and flakes surrounded by epoxy resin are in point contact with the PCMO surface.[21] On the basis of this model, it is thought that the properties of the point-contact Ag/LCMO interface such as contact area and AlO_x surrounding Ag grain have a great influence on the resistance switching properties of Ag–Al alloy/LCMO/Pt structures. The Al-33%Ag TE structure shows lower pulse voltage (±5 V) and shorter pulse width (100 ns) than those of Al-50%Ag TE structure,[18] which may be attributed to the different contact state of Ag–Al alloy/LCMO interface. As seen in Table 1, the resistance value of HRS and LRS of Al-33%Ag TE structure are significantly larger than those of Al-50%Ag TE structure, which also suggests that the effective area of Ag/LCMO memory cell was reduced in Al-33%Ag TE structure. Such reducing memory cell area for the point-contact Ag/LCMO interface will facilitate the switching operation. Therefore, to some extent, the switching speed can be improved in Al–Ag alloy/LCMO/Pt structures by decreasing the Ag content. To further improve the RS performance, however, more experiments need to optimize the Ag content.

4. Summary

In conclusion, we found that RS capability can be greatly improved by combining LCMO with Al-33%Ag alloy electrode. The switching properties and the RS mechanism were successfully explained by a model of the formation of Ag-contained AlO_x layer.

Acknowledgements This work is sponsored by the Ministry of Science and Technology of China through the Hi-Tech Research and Development program of China (Grant no. 2006AA03Z308), National Natural Science Foundation of China (No. 50672116), Shanghai-AM Research and Development Fund (No. 08700740900), Nature Science Foundation of Shanghai (No. 08ZR1421500), and Keystone Project of Shanghai Basic Research Program (No. 08JC1420600).

References

1) C. Yoshida, K. Tsunoda, H. Noshiro and Y. Sugiyama, *Appl. Phys. Lett.*, 91, 223510 (2007).
2) I. G. Baek, M. S. Lee, S. Seo, M. J. Lee, D. H. Seo, D.-S. Suh, J. C. Park, S. O. Park, H. S. Kim, I. K. Yoo, U-In. Chung and J. T. Moon, *Tech. Dig. IEDM*, 587–590 (2004).
3) W. W. Zhuang, W. Pan, B. D. Ulrich, J. J. Lee, L. Stecker, A. Burmaster, D. R. Evans, S. T. Hsu, M. Tajiri, A. Shimaoka, K. Inoue, T. Naka, N. Awaya, K. Sakiyarma, Y. Wang, S. Q. Liu, N. J. Wu and A. Ignatiev, *Tech. Dig. IEDM*, 193–196 (2002).
4) S. Q. Liu, N. J. Wu and A. Ignatiev, *Appl. Phys. Lett.*, 76, 2749–2751 (2000).
5) D. S. Shang, Q. Wang, L. D. Chen, R. Dong, X. M. Li and W. Q. Zhang, *Phys. Rev. B*, 73, 245427 (2006).
6) R. Dong, W. F. Xiang, D. S. Lee, S. J. Oh, D. J. Seong, S. H.

Heo, H. J. Choi, M. J. Kwon, M. Chang, M. Jo, M. Hasan and H. Hwang, *Appl. Phys. Lett.*, **90**, 182118 (2007).
7) C. J. Kim, B. I. Kim and I. W. Chen, *Jpn. J. Appl. Phys.*, **44**, 1260–1261 (2005).
8) K. Shono, H. Kawano, T. Yokota and M. Gomi, *Appl. Phys. Express.*, **1**, 055002 (2008).
9) H. Kawano, K. Shono, T. Yokota and M. Gomi, *Appl. Phys. Express.*, **1**, 101901 (2008).
10) M. Hasan, R. Dong, H. J. Choi, D. S. Lee, D.-J. Seong, M. B. Pyun and H. Hwang, *Appl. Phys. Lett.*, **92**, 202102 (2008).
11) Q. Wang, D. S. Shang, Z. H. Wu, L. D. Chen and X. M. Li, *Appl. Phys. A*, **86**, 357–360 (2007).
12) A. Sawa, T. Fujii, M. Kawasaki and Y. Tokura, *Appl. Phys. Lett.*, **85**, 4073–4075 (2004).
13) A. Odagawa, H. Sato, I. H. Inoue, H. Akoh, M. Kawasaki, Y. Tokura, T. Kanno and H. Adachi, *Phys. Rev. B*, **70**, 224403 (2004).
14) Y. B. Nian, J. Strozier, N. J. Wu, X. Chen and A. Ignatiev, *Phys. Rev. Lett.*, **98**, 146403 (2007).
15) M. J. Rozenberg, I. H. Inoue and M. J. Sanchez, *Phys. Rev. Lett.*, **92**, 178302 (2004).
16) Ch. Jooss, J. Hoffmann, J. Fladerer, M. Ehrhardt, T. Beetz, L. Wu and Y. Zhu, *Phys. Rev. B*, **77**, 132409 (2008).
17) T. Harada, I. Ohkubo, K. Tsubouchi, H. Kumigashira, T. Ohnishi, M. Lippmaa, Y. Matsumoto, H. Koinuma and M. Oshima, *Appl. Phys. Lett.*, **92**, 222113 (2008).
18) W. D. Yu, X. M. Li, R. Yang, X. J. Liu, Q. Wang and L. D. Chen, *J. Phys. D: Appl. Phys.*, **41**, 215409 (2008).
19) Z. W. Xing, N. J. Wu and A. Ignatiev, *Appl. Phys. Lett.*, **91**, 052106 (2007).
20) D. S. Shang, L. D. Chen, Q. Wang, Z. H. Wu, W. Q. Zhang and X. M. Li, *J. Mater. Res.*, **23**, 302–307 (2008).
21) M. Fujimoto, H. Koyama, Y. Nishi and T. Suzuki, *Appl. Phys. Lett.*, **91**, 223504 (2007).